Rev.Adv.Mater.Sci. 5 (2003) 100-109

THERMODYNAMICS FOR NANOSYSTEMS: GRAIN AND PARTICLE-SIZE DEPENDENT PHASE DIAGRAMS

M.J. Mayo[1,2], A. Suresh[1,3] and W. D. Porter[4]

[1] Department of Materials Science and Engineering, The Pennsylvania State University, University Park, PA 16802, USA
[2] Currently adjunct to the University of Maryland, Dept. of Materials Engineering, Bldg. 090, College Park, MD 20742-2115, USA
[3]Currently at Analog Devices, Inc., 804 Woburn Street, Wilmington MA 01887, USA
[4]High Temperature Materials Laboratory, Oak Ridge National Laboratory, Oak Ridge, TN 37831, USA

Received: July 01, 2003

Abstract. Unusual phases are often observed in nanocrystalline materials; these are often assumed to be metastable phases produced by non-equilibrium synthesis techniques. The present analysis shows that, in fact, some such phases are stable, and their presence can be rigorously predicted by thermodynamics. Using dilatometry and high temperature differential scanning calorimetry (HTDSC) on zirconia samples with varying grain sizes and yttria content, we are able to show that the tetragonal-to- monoclinic phase transformation temperature varies linearly with inverse crystallite/grain size. This shift, which traverses hundreds of degrees, obeys a simple thermodynamic model that adds an interfacial energy term to the total free energy of the system. The relevant thermodynamic parameters, such as the change in volumetric enthalpy and entropy, change in surface enthalpy and entropy, and the interfacial energy and strain energy change involved in the transformation, are calculated from experiment. The result is an ability to redraw the Y_2O_3 - ZrO_2 phase diagram with crystallite/grain size as a third variable.

1. INTRODUCTION

With increasingly available data on the preparation of nanomaterials, it is becoming commonplace to observe unusual phases when “ordinary” materials are fabricated in nanocrystalline form. For example, $BaTiO_3$ [1-4] and $PbTiO_3$ [1,5], both nominally cubic, manifest themselves in the tetragonal phase when fabricated at small crystallite sizes. CdSe [6] and CdS [7,8] take on the rock salt structure, rather than their conventional wurtzite structure. Nanocrystalline titania appears primarily in the anatase phase, rather than its “stable” rutile phase [9-12]. A similar phenomenon is seen in yttria, normally cubic, which takes on the monoclinic phase in nanocrystal synthesis experiments [13,14]. Lastly, zirconia powders have been observed to be tetragonal even in the absence of so-called stabilizing agents (typically, yttria, ceria, or other dopants), if the grain size is refined to the nanometer realm [15-23].

For these fine-grained and fine particle systems, many competing theories have been extended to explain the presence of high temperature phases at low temperatures, including 1) lack of nucleation sites [6], 2) internal pressure due to particle curvature [14], and 3) surface energy difference between polymorphs [9], to name a few. The surface energy difference theory has been evoked to explain the presence of high temperature phases at room temperature in ceramic [4,24] (including zirconia) and metal [25] systems. It has also been used to explain the well-known shift in the melting point of metals with particle size [26]. The evidence presented in this paper speaks in favor of the surface energy difference theory, which can be used to calculate shifts in phase diagrams with crystallite/grain size.

Corresponding author: M.J. Mayo, e-mail: mmayo@nas.edu

2. EXPERIMENTAL PROCEDURE

Powders. Nanocrystalline zirconia powders were synthesized by chemical co-precipitation from the reaction of a zirconium oxychloride salt solution (containing added dissolved yttria, as needed) with ammonia according to the methodology of Reference [27]. Zirconia powders of the composition ZrO_2–*x* mol% Y_2O_3 were produced, with *x*=0, 0.5, 1 and 1.5. These will hereafter be referred to as 0YSZ, 0.5YSZ, 1YSZ and 1.5YSZ. The as-fabricated crystallite size was typically 8-13 nm, as determined by both BET surface area analysis [28] and x-ray line broadening using the Scherrer [29] relation. To create samples at varying crystallite sizes, powders were preheated to 1200 °C for varying lengths of time and cooled to room temperature prior to testing.

For testing, the heat-treated powders were heated in a Netzsch 404 (Paoli, PA) high temperature differential scanning calorimeter (HTDSC) at 40°C/min to a temperature not exceeding the prior heat treatment temperature of 1200 °C, then cooled at 10 °C/min. The monoclinic-to-tetragonal phase transformation was observed as an endothermic event on heating. Conversely, the tetragonal-to-monclinic phase transformation was observed as an exothermic event on cooling. For both the forward and reverse transformations, the HTDSC onset temperature was used to calculate the temperature associated with the phase transformation. Peak areas, divided by heating rate, yielded transformation enthalpies in J/g; however, the conversion to J/m^3 required multiplying by densities appropriate to each composition. These were taken as 5.8, 6.14, 6.13, and 6.1 g/cm^3, for the compositions 0YSZ, 0.5YSZ, 1 YSZ and 1.5YSZ, respectively [28]. Crystallite sizes were measured by field emission scanning electron microscopy (FESEM) using a Leo 1530 FE-SEM (Cambridge, UK). Crystallite sizes measured after the high temperature pre-treatment but before the test began were taken as the crystallite size for the monoclinic-to tetragonal transformation on heating; crystallite sizes measured after cooling in the HTDSC was complete were assigned to the reverse tetragonal to monoclinic transformation. The FESEM-measured mean linear intercept crystallite sizes for free powders were corrected by a factor of 1.46 to yield true crystallite diameters.

Pellets. For studies on pellets, the as-produced (but not 1200 °C heat-treated) 0.5YSZ, 1.0YSZ and 1.5YSZ nanocrystalline powders were uniaxially pressed to 1.12 GPa and then sintered for 5 hours at 1040, 1060, and 1125 °C for the three compositions respectively. These time-temperature protocols yielded pellets of near single phase (>92% tetragonal) grains and densities of 93, 99 and 98% of theoretical. For pellets, only the tetragonal-to-monoclinic transformation on cooling was measured. Unfortunately, once monoclinic grains are created in previously tetragonal-grained pellet, the sample disintegrates into a powder, so it is not possible to measure the reverse $m \rightarrow t$ tranformation by reheating transformed pellets. It is equally impossible to begin studies using pellets sintered in the monoclinic phase, since any such pellets would by definition have a transformation temperature below room temperature; i.e., a transformation undetectable by HTDSC or conventional dilatometry.

For pellets, dilatometry (Theta Dilamatic II, Port Washington, NY) rather than HTDSC was used to measure the onset temperature for the $t \rightarrow m$ transformation on cooling. Each pellet was first preheated in the dilatometer at 1200 °C for varying lengths of time in the tetragonal phase field to achieve the grain size of interest. Samples were then cooled in situ at a rate of 10 °C/min. The sudden linear expansion event experienced on cooling was taken to be the tetragonal-to-monoclinic phase transformation, a dilatant transformation [30]. The grain size associated with the transformation on cooling was taken to be the FESEM-measured mean linear intercept grain sizes of the polished pellet surface after cooling was complete, multiplied by a factor of 1.56 to yield a true grain diameter.

3. RESULTS AND DISCUSSION

Observation of Phase Transformation on Heating (HTDSC). During the powder HTDSC runs, it was noted that the onset temperature for the phase transformation remained virtually identical on heating, but varied systematically with grain size on cooling. The heating result was attributed to a high density of twin interfaces present in room temperature (monoclinic) powders, which tended to make the “apparent” grain size (distance between interfaces) equal in all the samples, and hence result in transformation temperatures that were identical across all samples. This hypothesis was supported the fact that that x-ray line broadening measurements of samples at room temperature always gave a very small grain size of 50 nm, which was identical across all samples, while FESEM measurements of the same samples showed a systematic increase in grain size from (smallest = 120 nm) to (largest = 400 nm) with increasing time and temperature of heat treatment. After heating in the HTDSC (prior to cooling), these twins would presumably have an-

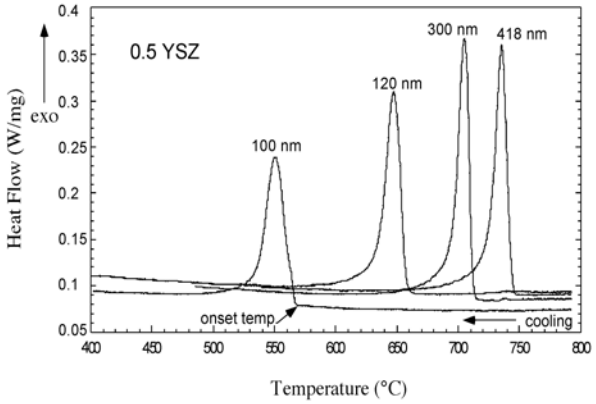

Fig. 1. Sample HTDSC data for 0.5 YSZ powder samples of varying crystallite size. The onset temperature in the cooling direction is shown for the 100 nm sample.

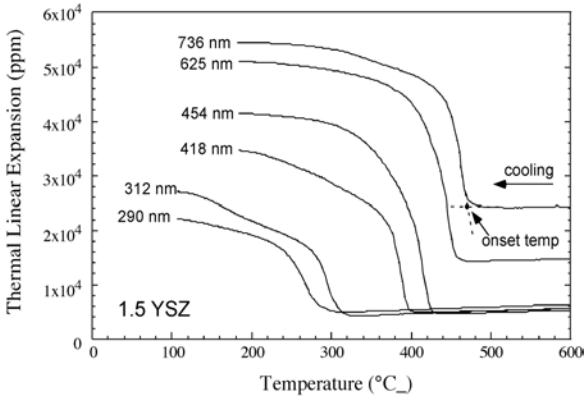

Fig. 2. Sample dilatometry data for 1.5 YSZ pellet samples. The onset temperature on cooling is shown for the 635 nm sample.

nealed out, which would explain why the transformation event on cooling was not driven by the twin spacing. Because differing transformation temperatures could be obtained only on cooling, the remainder of this discussion deals with the relationship between grain size and the transformation temperatures measured on cooling only, i.e., measurements of the shift of the upper boundary of the T+M (tetragonal + monoclinic) phase field. The T+M phase field is situated just below the single phase T field on the zirconia-yttria phase diagram [31]. Thus, the T/T+M boundary is where the tetragonal phase just begins to transform to the monoclinic phase on cooling.

Observation of Phase Transformation on Cooling (HTDSC and Dilatometry). A systematic decrease in tetragonal-to-monoclinic transformation temperature with decreasing crystallite/grain size was observed on cooling in both HTDSC and dilatometry experiments. Sample data for the two techniques are shown in Figs. 1 and 2, respectively. From the onset temperatures in these data, it is possible to plot the inverse crystallite (for powders) or grain (for pellets) size of the material vs. the temperature at which it transformed. The result (Fig. 3) is a linear relation for all compositions, whether pellets or powders. All samples exhibit the lower transformation temperatures – equivalent to increasing tetragonal phase stability – with smaller grain/particle sizes. The most plausible reason for this phenomenon is a lower surface/interfacial energy of the tetragonal zirconia compared to the monoclinic zirconia. For 0YSZ powders, this can be verified: the surface energy of the tetragonal phase is known to be about two thirds that of the monoclinic phase (γ_m = 1.13 J/m^2 and γ_t = 0.77 J/m^2; Refs. [20,32]). Assuming the trend is true of other compositions as well, the tetragonal phase should always be favored at very small crystallite/grain sizes, or, equivalently, large surface/interfacial areas. Garvie [16,17] and Lange [33] used this simple thermodynamic approach to explain why, in zirconia, the tetragonal phase appeared to be stabilized even down to room temperature in sufficiently fine powder crystallites. Here we show that a surface energy contribution can not only predict the observed inverse linear relation between grain/particle size and transformation temperature – but the values of many relevant thermodynamic constants as well.

Thermodynamic Approach and Formulation. *Powders.* At the point of transformation, the free energies of the monoclinic and tetragonal phases should be equal. For each phase,the free energy is composed of three parts: (1) a term due to the volume free energy, (2) a term due to the surface free energy, and (3) a term due to the elastic compression of the solid under the pressure exerted by the curved surface (LaPlace pressure, equal to surface energy times curvature). This last term was not considered in Garvie's work, and some experimental measurements throw into doubt its applicability to zirconia [20], but its inclusion in the derivation has the advantage of ultimately yielding more accurate predictions of surface energies and surface entropies. Therefore, assuming spherical particles, we have:

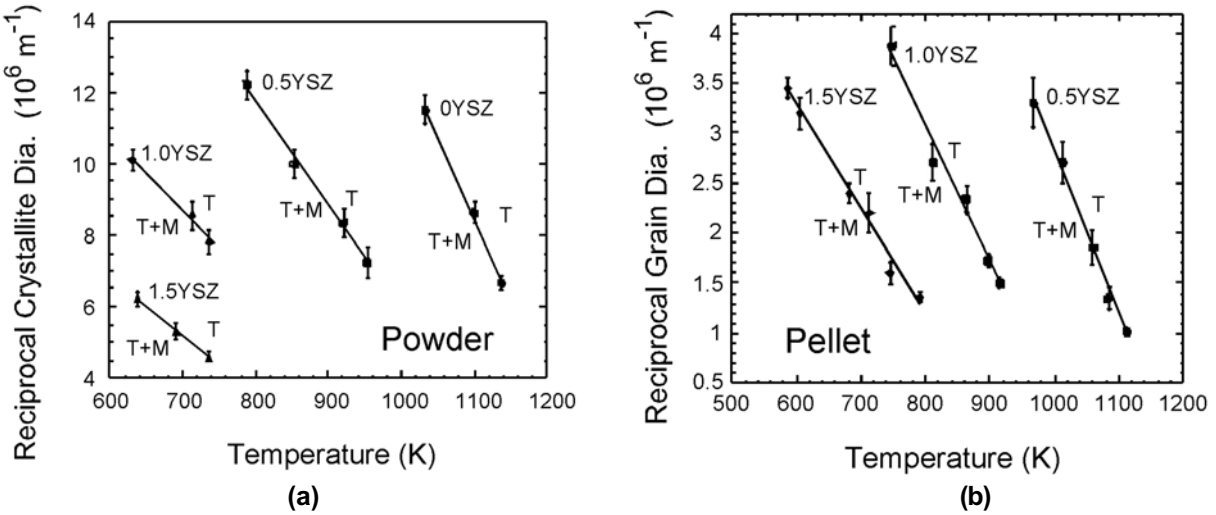

Fig. 3. Inverse critical crystallite/grain size versus transformation temperature for a) powders and b) pellets.

$$\Delta G_{t\to m} = G_m - G_t = \left(\frac{1}{6}\pi D^3 G_{vol,m} + \pi D^2 \gamma_m + \frac{1}{6}\pi D^3\left[\frac{4}{D}\gamma_m\right]\right) - \left(\frac{1}{6}\pi D^3 G_{vol,t} + \pi D^2 \gamma_t + \frac{1}{6}\pi D^3\left[\frac{4}{D}\gamma_t\right]\right) = 0. \quad (1)$$

Here, the subscript "vol" is intended to convey parameters that relate to the volume or bulk, that is, to the chemistry and lattice bonds of the system, not to its surfaces or interfaces. Thus, G_{vol} is the volumetric free energy of the tetragonal (t) and monoclinic (m) crystallites (also known as the chemical free energy); D is the crystallite size; and γ is the surface energy. Eq. 1 assumes no volume change during the phase transformation (D is the same for both phases). In reality, there is a volume change of 4%. If the "volume effects" are carried through all related terms in Eq. 1, the result is an extra set of terms that represents about 5% of the value of the surface energy terms already in Eq. 1. Volume change effects are therefore ignored in the derivation for the present material. The volumetric free energy, G_{vol}, can also be written as

$$G_{vol} = H_{vol} - TS_{vol}\ , \quad (2)$$

where T is the temperature in degrees Kelvin, and H_{vol} and S_{vol} are the enthalpy and entropy, respectively, for an infinite crystal at temperature. Substituting Eq. 2 in Eq. 1 for each phase, setting $\Delta G_{t\to m}$ =0, and rearranging the terms leads to:

$$D^* = \frac{10(\gamma_m - \gamma_t)}{G_{vol,t} - G_{vol,m}} = \frac{10\Delta\gamma_{t\to m}}{-\Delta H_{vol,t\to m} + T\Delta S_{vol,t\to m}}. \quad (3)$$

In Eq. 3, D^* is the grain size at which a material will spontaneously transform from the tetragonal to the monoclinic phase. D^* will vary with composition (primarily captured in the ΔH_{vol} and ΔS_{vol} terms) and temperature. Assuming that $\Delta G_{vol} = \Delta H_{vol} - T\Delta S_{vol} = 0$ at $T = T_b$, the following useful substitution for $\Delta S_{vol,t\to m}$ can also be made:

$$\Delta S_{vol,t\to m} = \frac{\Delta H_{vol,t\to m}}{T_b}. \quad (4)$$

At this point, the relationship between the tetragonal → monoclinic transformation temperature and the crystallite size can be written as,

$$\frac{1}{D^*} = \frac{\Delta H_{vol} T}{10\Delta\gamma T_b} - \frac{\Delta H_{vol}}{10\Delta\gamma} \quad \text{for powders.} \quad (5)$$

Elimination of the t→m subscript in the enthalpy and entropy terms reflects the fact that these parameters are already in the proper direction to be compatible with what would be measured in a cooling experiment.

An analogous expression for pellets can be derived:

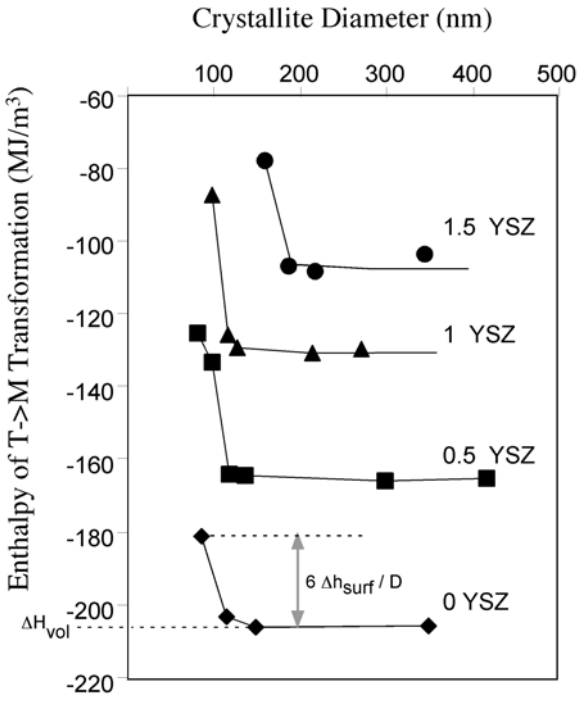

Fig. 4. Enthalpy of the tetragonal-to-monoclinic phase transformation in the HTDSC powder samples, plotted as a function of grain size. Sample calculations for ΔH_{vol} and Δh_{surf} are shown on the 0YSZ curve.

$$\frac{1}{D^*} = \frac{\Delta H_{vol} T}{10 \Delta\Sigma T_b} - \frac{\Delta H_{vol} + \Delta U_{se}}{10 \Delta\Sigma} \quad \text{for pellets.} \qquad (6)$$

In Eq. 6, $\Delta\Sigma$ is the interfacial (primarily grain boundary) energy difference between the monoclinic and the tetragonal phase. The expression for pellets also contains the term ΔU_{se}, which is the strain energy involved in the transformation. For pellets, the transforming grain is embedded in a matrix. When the transforming grain undergoes the volume increase associated with the conversion to the monoclinic phase, either the surrounding tetragonal matrix or the grain itself has to elastically deform in order to accommodate the resulting geometric mismatch. The requirement for geometric compatibility leads to the additional strain energy term [34]. As alluded to earlier, this extra term is one reason why the same material (composition) gives different transformation temperatures in the pellet form vs. the powder form. Generally, the pellets retain the tetragonal phase to much lower temperatures than do the powders. This point is evident in comparing Fig. 3b to Fig. 3a.

Enthalpies, Entropies, and Energies of the Phase Transformation in Powders. *Volumetric Enthalpy and Surface Enthalpy: Powder Data.* In addition to providing information on transformation temperatures, the HTDSC powder experiments (but not the dilatometry pellet experiments) yield enthalpy values for the transformation. The data show that transformation enthalpies remain at a constant value for each composition for all large crystallite sizes (see Fig. 4). This plateau enthalpy, of course, corresponds to the enthalpy for an infinitely large particle, or ΔH_{vol}. But, at some crystallite size below 200 nm, the measured enthalpy progressively diminishes in magnitude, suggesting that the total enthalpy is not just ΔH_{vol}, but ΔH_{vol} plus some enthalpy contribution of opposite sign. Because this second component becomes larger as crystallite size decreases, we tentatively attribute the second component of the total measured enthalpy to the surface enthalpy, which would then be opposite in sign to the volumetric enthalpy. Thus,

$$\Delta H_{meas} = \frac{6}{D} \cdot \Delta h_{surf} + \Delta H_{vol}\,, \qquad (7)$$

where Δh_{surf} is the difference in surface enthalpy between the two phases (in J/m^2), and the multiplicative factor of 6/D is applied to convert the surface enthalpy contribution to a per unit volume basis. In practice, we can obtain Δh_{surf} only from data that fall far from the enthalpy plateau, i.e., where there is a significant difference between ΔH_{meas} and the

Table 1. Volumetric thermodynamic parameters governing the tetragonal (t) and monoclinic (m) phase stability in powders and pellets. All parameters preceded by "Δ" take the monoclinic state as the final state and the tetragonal state as the initial state; i.e., they represent the subtraction of the tetragonal value from the monoclinic value.

	Volumetric Parameters (Powders and Pellets)		
	T_b (K)	ΔH_{vol} x 10^6 (J/m^{3}K)	ΔS_{vol} x 10^3 (J/m^3)
0YSZ	1286	-205.3	-159.7
0.5YSZ	1201	-164.5	-136.9
1.0YSZ	1119	-129.3	-115.5
1.5YSZ	1012	-105.6	-104.3

Table 2. Thermodynamic parameters specific to surfaces (in powders), interfaces (in pellets) and strain energy (relevant to pellets only). The surface/interfacial parameters are responsible for the crystallite/grain size dependence of tetragonal (t) to monoclinic (m) phase transformation in powders and pellets. The strain energy term is largely responsible for the difference in transformation temperatures between powders and pellets. All parameters preceded by "Δ" take the monoclinic state as the final state and the tetragonal state as the initial state; i.e., they represent the subtraction of the tetragonal value from the monoclinic value.

	I. Powders				*II. Pellets*	
	$\Delta\gamma$ (J/m^2) (at avg. transf. temp) [avg. transf. temp, K]	Δh_{surf} (J/m^2)	Δs_{surf} (mJ/m^2K)	$\Delta\gamma$ (J/m^2) (at RT)	$\Delta\Sigma$ (J/m^2) (at avg. transf. temp) [avg. transf. temp, K]	ΔU_{se} (J/m^3)
0YSZ	0.350 [1090]	0.359	0.008	0.357	N/A	N/A
0.5YSZ	0.468 [879]	0.545	0.098	0.525	0.834 [1047]	$4.04x10^6$
1.0YSZ	0.558 [693]	0.706	0.235	0.651	0.844 [847]	$1.09x10^7$
1.5YSZ	0.629 [688]	0.761	0.206	0.709	0.997 [687]	$1.033x10^7$

plateau enthalpy of ΔH_{vol}. Although the existence of a Δh_{surf} is purely an assumption of the present paper, this assumption does lead to expressions for other thermodynamic variables whose numerical values can be independently verified from the literature (see the section of this paper entitled "Check of Thermodynamic Parameters"). Thus, it seems likely that the observation of decreasingly exothermic tetragonal-to-monoclinic phase transformations is, in fact,the result of an endothermic surface enthalpy contribution. Values of ΔH_{vol} and Δh_{surf} are tabulated in Tables 1 and 2.

Surface Energy, Surface Entropy, Volumetric Entropy and Bulk Transformation Temperature: Powder Data. If the second, detractive component of enthalpy is a true surface enthalpy, then it should also be observable as a component of the surface *energy* difference, $\Delta\gamma$, between the two phases, according to

$$\Delta\gamma = \Delta h_{surf} - T\Delta s_{surf}\,, \tag{8}$$

where Δs_{surf} would be the surface entropy, or the temperature-dependent component of the surface energy. According to Eq. 5, a plot of $1/D^*$ (inverse sample crystallite size at transformation) vs. T (transformation temperature) gives $-\Delta H_{vol}/10\Delta\gamma$ as its intercept.,

$$\Delta\gamma = -\frac{\Delta H_{vol}}{\text{intercept}\cdot 10}\,, \tag{9}$$

where ΔH_{vol} is already known from the plateau enthalpies of Fig. 4. It should be stressed that surface energy differences calculated in this way yield the value at the transformation temperature, not at room temperature.

With $\Delta\gamma$ and Δh_{surf}^* now known, Δs_{surf} can be calculated at the temperature of transformation according to Eq. 8. Since Δs_{surf} does not itself change with temperature (with any degree of significance), Δs_{surf} can now also be used to extrapolate the high temperature values of $\Delta\gamma$ to room temperature – again using Eq. 8.

Another thermodynamic parameter obtainable from the HTDSC experiments is T_b, the transformation temperature for an infinite crystal. It is calculated from the ratio of the slope to the intercept (see Eq. 5), using each composition's plot of $1/D^*$ vs. T:

$$T_b = \frac{\text{intercept}}{\text{slope}}\,. \tag{10}$$

Finally, ΔS_{vol} can be calculated as the ratio of ΔH_{vol} to T_b (see Eq. 4), now that T_b is known.

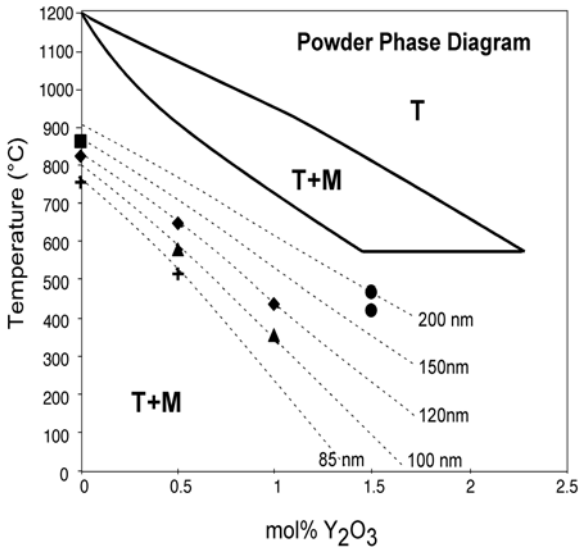

Fig. 5. Movement of the T→T+TM phase boundary to lower temperatures with decreasing crystallite size in powders. Dashed lines represent the solutions of Eq. 13 for different values of *D*. Data points represent measured transformation temperatures in HTDSC experiments on powders whose crystallite size happened to be close to 85, 100, 120, 150, or 200 nm. Solid lines are the equilibrium phase diagram for (large-grained) solids, taken from Ref. [31].

Values of $\Delta\gamma$ (at transformation temperature), $\Delta\gamma$ (at room temperature), Δs_{surf}, ΔS_{vol}, and T_b are given in Tables 1 and 2.

Critical Crystallite Size: Powder Data. Though not strictly a thermodynamic parameter, is often of interest to determine the critical crystallite size at room temperature, D_{RT}. Below this crystallite size, a powder will always be observed in the tetragonal form (at least, for all observations above room temperature), even though the "normal," "expected" phase for zirconia is the monoclinic phase. It was some of these earlier observations of the unexpected tetragonal phase in fine zirconia powders that led to the original inquiries into crystallite size stabilization [17,18]. For this calculation, one solves first for D^* by setting ΔG=0, remembering that ΔG has both a surface and volume component:

$$\Delta G = \Delta G_{vol} + \frac{10}{D}\Delta\gamma = \left(\Delta H_{vol} - T\Delta S_{vol}\right) + \frac{10}{D}\left(\Delta h_{surf} - T\Delta s_{surf}\right) = 0. \quad (11)$$

Upon rearranging, Eq. 11 yields:

$$D^* = \frac{-10\cdot\left(\Delta h_{surf} - T\Delta s_{surf}\right)}{\Delta H_{vol} - T\Delta S_{vol}}. \quad (12)$$

At 298K, Eq. 12 predicts critical crystallite diameters of 22.6, 41.7, 67 and 93.8 nm for the 0YSZ, 0.5YSZ, 1YSZ, and 1.5 YSZ powder compositions, respectively.

Crystallite Size Dependent Phase Diagrams for Powders. A slight rearrangement of Eq. 12 enables one to plot the shift in transformation temperature with crystallite size as a moving phase boundary on a conventional phase diagram:

$$T_{transform} = \frac{\Delta H_{vol} + \frac{10\Delta h_{surf}}{D^*}}{\Delta S_{vol} + \frac{10\Delta s_{surf}}{D^*}}. \quad (13)$$

To plot Eq. 13 in temperature-composition space, it is necessary to assign composition dependencies to all thermodynamic variables; this can be done by quadratic or linear fits to the existing composition-dependent values in Tables 1 and 2. The resulting plot of transformation temperature vs. composition, for different fixed values of crystallite size, is shown in Fig. 5.

Enthalpies, Entropies, and Energies of the Phase Transformation in Pellets. For pellets, it is assumed that all of the *volumetric* parameters remain the same as in the powders. That is, ΔH_{vol}, ΔS_{vol} and T_b are considered to be the same for an infinitely large grain in a pellet, as for an infinitely large free crystal. However, the pellets have two thermodynamic terms the powders do not have. Instead of a surface energy difference between two phases. $\Delta\gamma$, the pellets have an interfacial energy difference, $\Delta\Sigma$. In practice, this term comprises all interfacial energy contributions, including not only those of grain boundaries, but of twins and microcracks as well. Pellets also have the term ΔU_{se}, which the reader will recall is the strain energy involved in the transformation.

A plot of pellet transformation temperatures showing $1/D^*$ vs. T will, according to Eq. 6 yield a slope of $\Delta H_{vol}/(10\Delta\Sigma T_b)$. The volumetric parameters ΔH_{vol} and T_b are known from the prior HTDSC data, leaving it easy to extract the value of $\Delta\Sigma$. The intercept of the same plot yields $(\Delta H_{vol}+U_{se})/10\Delta\Sigma$, which can be decoded to yield ΔU_{se}, now that the other parameters are known.

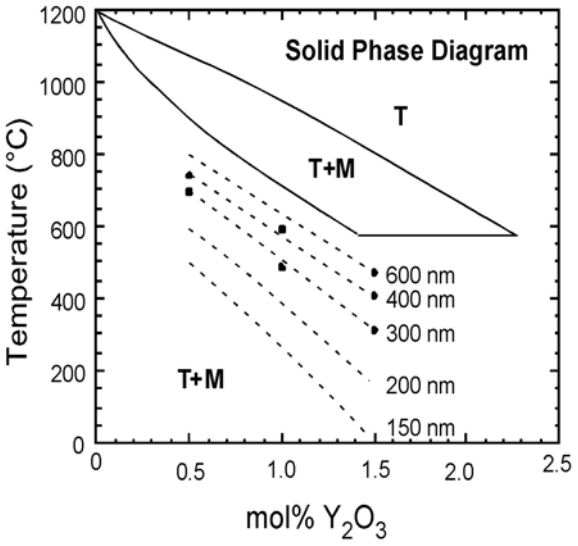

Fig. 6. Grain-size dependent phase diagram, obtained by linear interpolation between lines in Fig. 3(b) (does not include interfacial entropy effects). Solid lines are from the zirconia rich side of a standard ZrO_2–Y_2O_3 phase diagram [31]. Dotted lines represent the shift in the upper phase boundary for each grain size. T and M stand for tetragonal and monoclinic respectively. (•) represents actual data points from the dilatometer runs.

Grain Size Dependent Phase Diagrams for Pellets. To accurately calculate a grain size dependent phase diagram for pellets requires knowing the interfacial counterparts to Δh_{surf} and Δs_{surf}, i.e. surface enthalpy and surface entropy components of the interfacial energy, Δh_{int} and Δs_{int}. These parameters can theoretically be obtained from calorimetry experiments on pellets, but they were not obtained in the present dilatometry experiments. Without these parameters, the pellet parallel to Eq. 13 cannot be calculated. However, an approximate grain-size dependent phase diagram can still be constructed from the existing data by drawing constant grain size lines across Fig. 3b to obtain three temperature-composition data pairs for each grain size. The composition dependence of the transformation temperature at that grain size can then be determined by linear interpolation. The resulting phase diagram, though not accurate outside the bounds of the collected data, still gives a good sense of the downward movement of the T/T+M phase boundary with decreasing grain size (Fig. 6).

Check of Thermodynamic Parameters. The thermodynamic framework presented in Eqs. 1-13 is untested. However, it has the advantage of giving numerical values for a number of thermodynamic parameters, some of which have already been observed and reported in the literature. Thus, a comparison with literature values, where they exist, should indicate whether the present approach is sound.

Ref [32] reports the value of $\Delta\gamma$ for 0YSZ powders to be 0.36 J/m^2 at room temperature, based on experimental measurements of heats of immersion. The present estimate, at $\Delta\gamma$=0.357 J/m2, is nearly identical. For the powder case, there are also past observations of powders that are monoclinic above a certain size, but tetragonal below a certain size, for the 0YSZ composition. These experimental observations would put the 0YSZ room temperature critical crystallite size at 18 nm (transmission electron microscopy, Ref. [20]) or 20 nm (heat of immersion measurements, Ref. [16]). The present study obtains a D^*_{RT} of 22.6 nm for 0YSZ powders.

Some of the thermodynamic parameters derived herein are not known experimentally but can be tested for general reasonableness. For instance, for each phase, the interfacial energy can be no more than twice the surface energy of that phase; otherwise it would be thermodynamically favorable for the material to always remain in powder form (pellets could not be made at any temperature; they would spontaneously disintegrate into powders). The *difference* between the two phases' interfacial energies , $\Delta\Sigma$, must therefore also be less than twice the interfacial energy *difference*, $\Delta\gamma$. This test is passed : $\Delta\Sigma \sim 0.46$ to $0.53 \times 2\Delta\gamma$ for each composition tested. However, it should also be noted that in the present case, $\Delta\Sigma$ may contain contributions from twin and microcrack energies also. Finally, the strain energy difference, ΔU_{se} – here estimated from thermodynamic considerations – should also be reasonable from a mechanical point of view. Treating the material as a spring, we roughly estimate the strain energy as equal to the stress times the strain, or

$$\Delta U_{se} \approx \sigma\varepsilon = 0.5E\varepsilon^2, \qquad (14)$$

where ε is the strain involved in the transformation and E is the modulus of the material. For zirconia, a modulus of 160 GPa is assumed [32,35], and the linear strain can be estimated from the dilatometry data as 1.48% for almost all compositions. This yields a dilatational strain energy of 1.77×10^7 J/m^3, while ΔU_{se} from the thermodynamic framework is between 0.4×10^7 to 1.1×10^7 J/m^3, for the three com-

positions tested. The measured values will not coincide exactly with the calculation of Eq. 14 for several reasons. First, they contain shear contributions (which can be either positive or negative) as well as the dilatational contributions of Eq. 14; secondly, the actual modulus of some samples may be lower than that presumed, due the presence of small cracks or voids. For very small cracks of high aspect ratio, the material modulus may be decreased in fact by up to 80% [36].

Thus, with some degree of outside confirmation, it appears that a wide range of thermodynamic parameters, as listed in Tables 1 and 2, can be obtained from very straightforward HTDSC and dilatometry scans – and that these parameters have some basis in reality.

One Application of the Grain/Particle Size Dependent Phase Diagram. Previous experimental work on the fracture toughness of yttria doped zirconia has suggested that fracture toughness could be increased by up to a factor of 5, if the ceramic's grain size, composition, and temperature were carefully adjusted to place the ceramic just barely on the tetragonal edge of the tetragonal-to-monoclinic phase transformation condition [38]. Interpreting this finding in light of the present thermodynamic data, we see that the lines in Fig. 3(b) correspond to critical grain sizes in solid samples, so theoretically, staying just barely on the single phase tetragonal side of these lines would represent the combination of yttria content and grain size to attain maximum fracture toughness at any temperature along the line. Since room temperature is the most common service temperature for many materials, the critical grain size at room temperature, D^*_{RT} is especially important. For powders, D^*_{RT} can be determined strictly thermodynamically, from Eq. 13. For pellets, the necessary counterparts to surface enthalpy and surface entropy terms – interfacial enthlapy and interfacial entropy – are not available from the present study, because pellet data were obtained by dilatometry instead of HTDSC. As a rough estimate, we can extrapolate the lines in Fig. 3(b) to 298K in order to calculate the critical grain size at room temperature. This estimate yields D^*_{RT} to be 70 nm, 100 nm, 155 nm for 0.5YSZ, 1.0YSZ and 1.5YSZ respectively. These grain sizes are reasonably close to those where maximum toughness was observed at room temperature in the fracture toughness study [38]: 90 nm and 110 nm for 1.0YSZ and 1.5YSZ, respectively. Some discrepancy is further expected, since grain diameters were measured by different methods in the two studies: FESEM in the present case, x-ray line broadening in the study of Ref. [38]. The x-ray line broadening technique, in particular, becomes increasingly less reliable above 100 nm.

4. CONCLUSION

High temperature differential scanning calorimetry (HTDSC) and dilatometry can be used to extract the thermodynamic data regulating the tetragonal-to-monoclinic transformation in nanocrystalline and submicron yttria-doped zirconia powders and pellets. These data show the transformation temperature can be lowered hundreds of degrees by manipulation of the crystallite (in powders) or grain (in pellets) size. The data in both powder and pellet cases exhibit an inverse linear relationship between grain/crystallite size and transformation temperature, as predicted a simple thermodynamic model in which surface (or interfacial) energy terms are added to the overall free energy of the system. The large and systematic shift of transformation temperature with grain size requires the yttria-zirconia phase diagram to be redrawn, incorporating grain size as a third variable. Powder and pellet phase diagrams are necessarily different, partly because of the larger numerical value of interfacial energy compared to surface energy, but primarily because of the extra strain energy term that enters the thermodynamic formulation in the pellet case.

The HTDSC experiments are found to be especially useful in yielding plentiful thermodynamic information on the grain size-dependent transformation. From simple HTDSC scans one can obtain the volumetric enthalpy and entropy of transformation, the bulk transformation temperature; and the surface energy, enthalpy, and entropy differences between the tetragonal and monoclinic phases. Dilatomatry data on pellets additionally yield an estimate of the interfacial energy difference between the tetragonal and monoclinic phase, and the strain energy involved in the transformation. Unfortunately, dilatometry does not yield information on the interfacial enthalpy and entropy terms, which are needed to extend a theoretically accurate calculation of the yttria-zirconia diagram for solids all the way to room temperature.

ACKNOWLEDGEMENTS

This research was supported by the U. S. Department of Energy under contract No. DE-FG02-98ER45700 and the High Temperature Materials Laboratory User Program, Oak Ridge National Laboratory, managed by UT-Battelle, LLC, for the

U.S. Department of Energy under contract number DE-AC05-00OR22725. One of the authors (MM) would also like to thank Yuri Mishin of George Mason University for his compelling arguments that the LaPlace pressure was real and should not be ignored, despite failed attempts in the literature at measuring its effects in solids.

REFERENCES

[1] E.K. Akdogan, W. Mayo, A. Safari, C.J. Rawn, and E.A. Payzant // *Ferroelectrics* **223** (1999) 11.
[2] M.H. Frey and D.A. Payne // *Phys. Rev. B* **54** (1996) 3158.
[3] B.D. Begg, E.R. Vance and J. Nowotny // *J. Am. Ceram. Soc* **77** (1982) 3186.
[4] S. Schlag, H-F. Eicke and W.B. Stern // *Ferroelectrics* **173** (1995) 351.
[5] G.A. Rossetti, J.P. Cline and A. Navrotsky // *J. Mater. Res.* **13** (1998) 3197.
[6] S.H. Tolbert and A.P. Alivisatos // *Science* **265** (1994) 273.
[7] A.P. Alivasatos // *Ber Bunsenges Phys. Chem.* **101** (1997) 1573.
[8] C-C. Chen, A.B. Herhold, C.S. Johnson and A.P. Alivisatos // *Science* **276** (1997) 398.
[9] H. Zhang and J.F. Banfield // *J. Mater. Chem.* **8** (1998) 2073.
[10] H. Zhang and J.F. Banfield, In: *Mater Res. Soc. Symp. Proc.* ***481***, ed. by E. Ma, P. Bellon, M. Atzmon and R. Trivedi (Warrendale, PA: MRS, 1998) p. 619.
[11] H. Zhang and J.F. Banfield // *J. Phys. Chem. B* **104** (2000) 3481.
[12] A.A. Gribb and J.F. Banfield // *Am. Miner.* **82** (1997) 717.
[13] H. Hahn, G. Skandan and J.C. Parker // *Scripta Metall. et Mater.* **25** (1991) 2389.
[14] G. Skandan, C.M. Foster, J. Frase, M.N. Ali and J.C. Parker // *Nanostruct. Mater* **1** (1992) 313.
[15] M. Winterer, R. Nitsche, S.A.T. Redfern, W.W. Schmahl and H. Hahn // *Nanostructured Materials* **5** (1995) 679.
[16] R.C. Garvie // *J. Phys. Chem.* **82** (1978) 218.
[17] R.C. Garvie and M.V. Swain // *J. Mater. Sci.* **20** (1985) 1193-1200.
[18] R.C. Garvie and M.C. Goss // *J. Mater. Sci.* **21** (1986) 1253.
[19] T. Chraska, A.H. King, C.C. Berndt and J. Karthikeyan // In: *Mater Res. Soc. Symp. Proc.* **481**, ed. by E. Ma, P. Bellon, M. Atzmon and R. Trivedi (Warrendale, PA: MRS, 1998) p. 613.
[20] T. Chraska, A.H. King and C.C. Berndt // *Mater. Sci. and Eng.* **A286** (2000) 169.
[21] G. Skandan, H. Hahn, M. Roddy and W.R. Cannnon // *J. Am. Ceram. Soc.* **77** (1994) 1706.
[22] R. Nitsche, M. Winterer and H. Hahn // *Nanostructured Materials* **6** (1995) 679.
[23] Z. Ji, J.A. Haynes, M.K. Ferber and J.M. Rigsbee // *Surface and Coatings Technology* **135** (2001) 109.
[24] J.M. McHale, A. Auroux, A.J. Perrotta and A. Navrotsky // *Science* **277** (1997) 788.
[25] R.P. Berman and A.E. Curzon // *Can. J. Phys.* **52** (1974) 923.
[26] A.N. Goldstein, C.M. Echer and A.P. Alivisatos // *Science* **256** (1992) 1425.
[27] M. 3iftэioglu and M.J. Mayo // In: *Mater Res. Soc. Symp. Proc.* **196**, ed. by M. Kobayashi, M. J. Mayo and J. Wadsworth (Pittsburgh, PA: MRS, 1990) p. 77.
[28] R.P. Ingel and D. Lewis III // *J. Am. Ceram. Soc.* **69** (1986) 325.
[29] H.P. Klug and L.E. Alexander, *X-ray Diffraction Procedures for Polycrystalline and Amorphous Materials* (New York: Wiley, 1974).
[30] R.J.H. Hannink // *Mater. Forum* **23** (1999) 153.
[31] H.G. Scott // *J. Mater. Sci* **10** (1975) 1527.
[32] I.W. Chen and Y.H. Chiao // *Acta Metall.* **31** (1983) 1627.
[33] F.F. Lange // *J. Mater Sci.* **17** (1982) 225.
[34] D.J. Green, R.J. H. Hannink and M.V. Swain, *Transformation Toughening of Ceramics* (Boca Raton, FL: CRC Press, 1988).
[35] W.Z. Zhu // *Ceram. Intl.* **22** (1996) 389.
[36] D.J. Holcomb and M.J. Mayo // *J. Mater. Res.* **5** (1990) 1827.
[37] E. Bernstein, M.G. Blanchin, R. Chapuis and R.J. Carvajal // *J. Mater. Sci* **27** (1992) 6519.
[38] Alfonso Bravo-Lйon, Yuichiro Morikawa, Masanori Kawahara and Merrilea J. Mayo // *Acta Materialia* **50** (2002) 4555.